Supporting Information

for *Small*, DOI: 10.1002/smll.201600326

Fiber-Shaped Perovskite Solar Cells with High Power Conversion Efficiency

*Longbin Qiu, Sisi He, Jiahua Yang, Jue Deng, and Huisheng Peng**

Supporting Information

Experimental Section

Synthesis of spinnable carbon nanotube (CNT) array and transparent CNT sheet electrode. The spinnable CNT array was synthesized through chemical vapor deposition process in a 2 inch furnace. A silicon wafer had been used as a substrate to sequentially deposit Al_2O_3 with a thickness of 3 nm and Fe with a thickness of 1.1 nm as the catalyst at the polished silicon surface. Ethylene (flowing rate of 90 sccm) was used as a carbon precursor. Hydrogen (flowing rate of 30 sccm) and argon (flowing rate of 400 sccm) was mixed as the carrier gas to grow CNT arrays for 10 min at 740 ^oC. The transparent CNT sheet was directly dry-drawn from the spinnable CNT array.

Synthesis of CH_3NH_3I. To synthesize the CH_3NH_3I, a hydroiodic acid aqueous solution (45 wt%, 12.5 mL) was firstly added to a methylamine/ethanol solution (6.4 wt%, 124 mL) at 0 ^oC under stirring for 2 h. The resulting solution was evaporated at 50 ℃ and then dissolved with hot ethanol. The following solution was precipitated by diethyl ether for three times to produce a white powder of methylamine iodide. This powder was kept in dark and under dry conditions before using.

Characterization. The structures were characterized by scanning electron microscopy (SEM, Hitachi FE-SEM S-4800 operated at 1 kV) and transmission electron microscopy (TEM, JEOL JEM-2100F operated at 200 kV). X-ray diffraction patterns were obtained from an X-ray powder diffractometer (D8 ADVANCE and DAVINCI.DESIGN). J-V curves were recorded by a Keithley 2420 Source Meter under illumination (100 mW/cm^2) of simulated AM1.5 solar light coming from a solar simulator (Oriel-Sol3A 94023A equipped with a 450 W Xe lamp and an AM1.5 filter). The EQE spectra were characterized by an IPCE measurement system (QTest Station1000D, Crowntech, Inc.). The Electrochemical Impedance spectra were performed on a CHI660a electrochemical workstation. XPS measurements were performed in Axis Ultra DLD from Kratos, equipped with a monochromatic Al KαX-ray source.

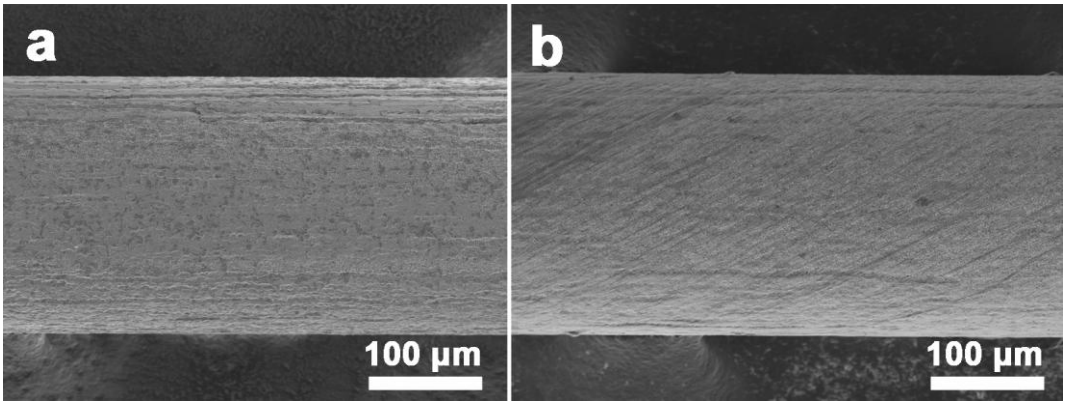

Figure S1. SEM images by a side view. **a)** A titanium wire. **b)** A PSCF.

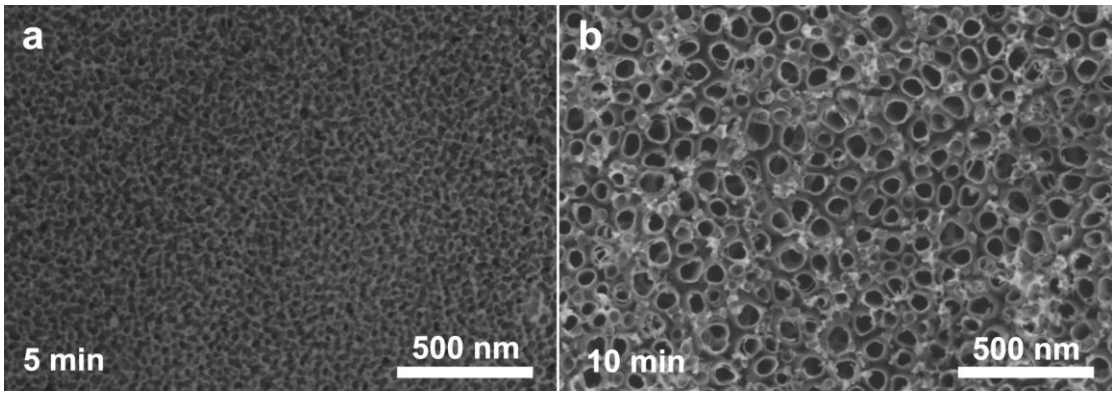

Figure S2. Structure evolution of aligned TiO_2 nanotubes during anodization for the different time at 20 V. **a)** 5 min; **b)** 10 min.

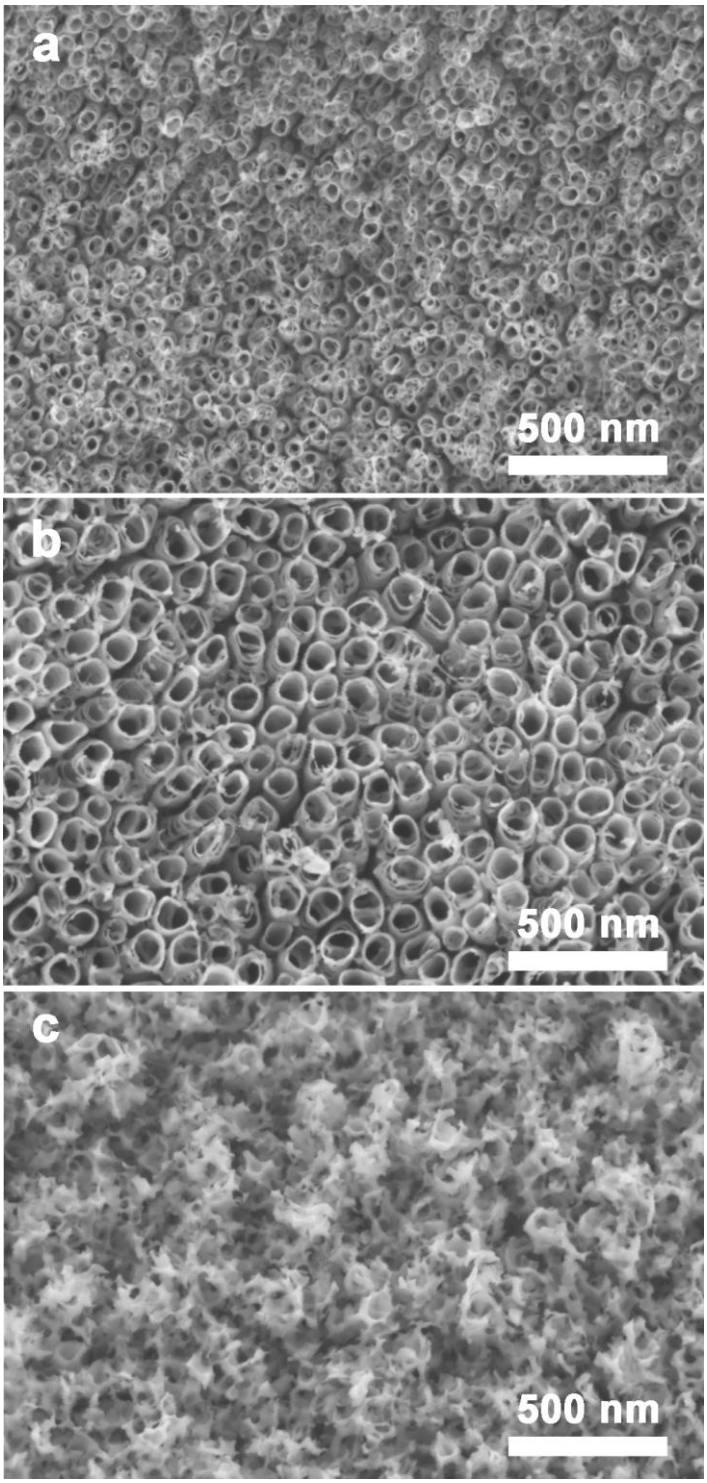

Figure S3. SEM images of titanium wires with increasing anodization voltages by a top view. **a)** 10 V. **b)** 20 V. **c)** 30 V.

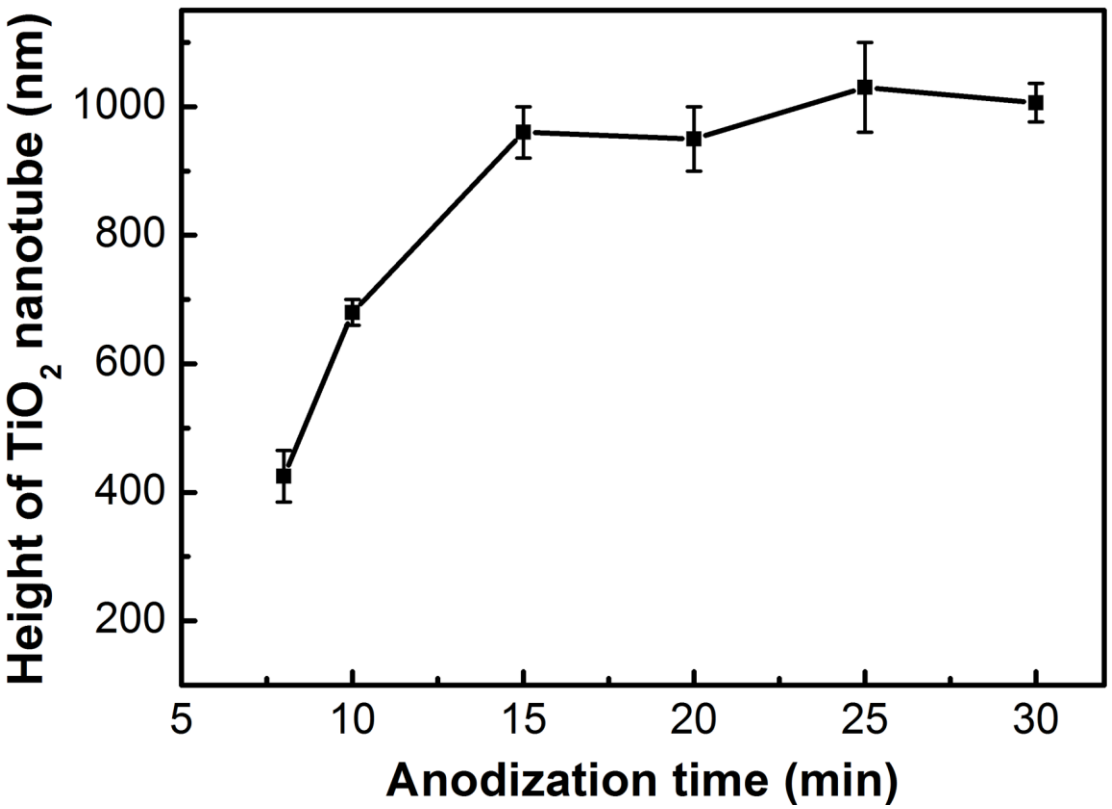

Figure S4. Growth of aligned TiO_2 nanotubes as a function of anodization time.

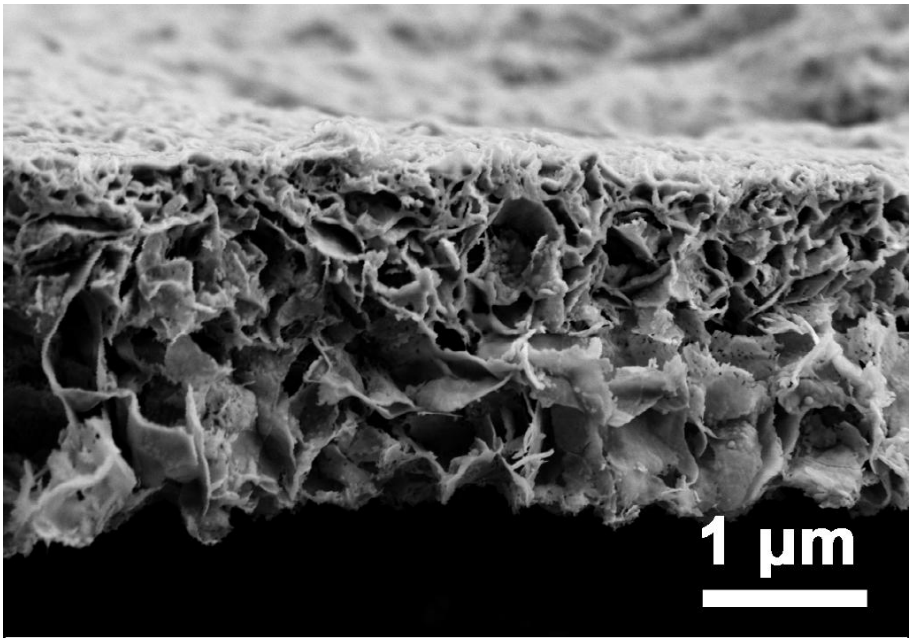

Figure S5. Porous lead oxide sponge formed by a cathodic electrodeposition.

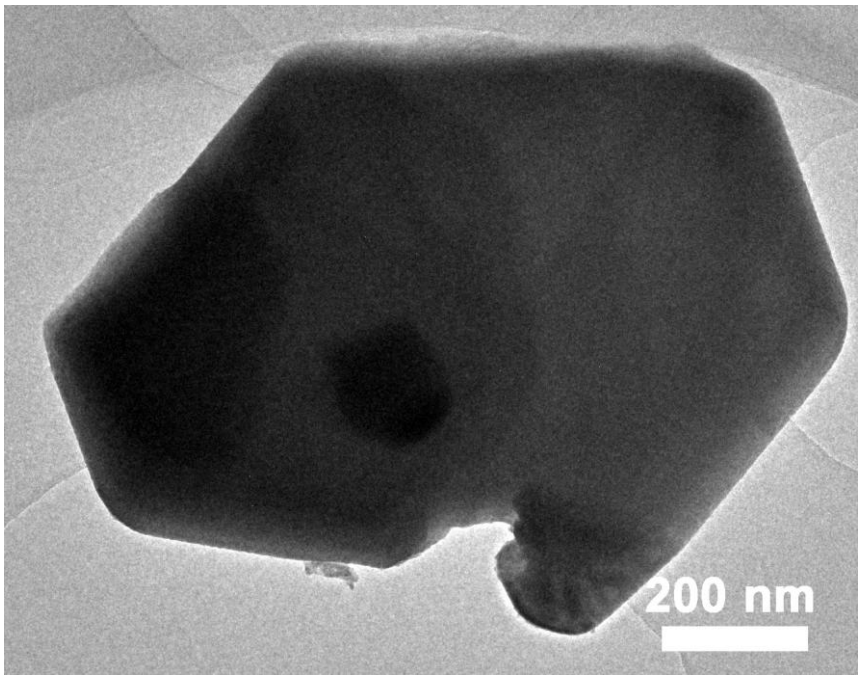

Figure S6. TEM image of a typical lead iodide structure through a cathodic deposition and reduction process by hydroiodide acid.

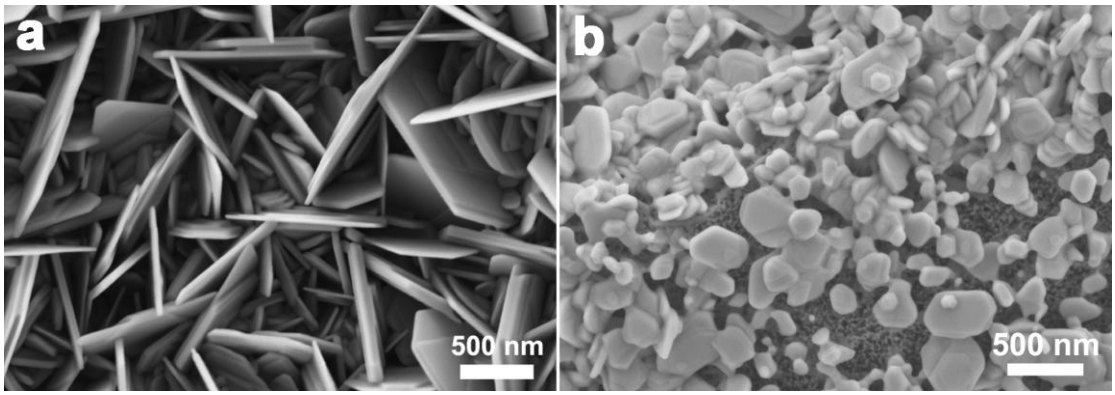

Figure S7. SEM images of lead iodide layers produced with different depositing densities. **a)** Dense nano-plate array reduced from a PbO layer with thickness of 2 μm. **b)** Sparse nano-plate layer reduced from a PbO layer with thickness of 100 nm.

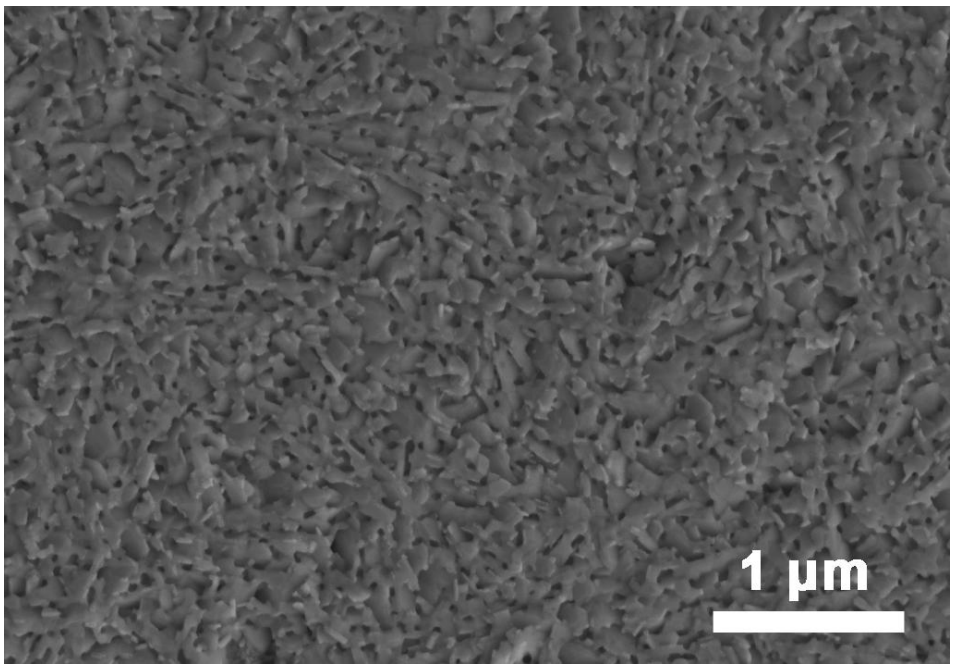

Figure S8. Surface morphology of a dense and flat lead iodide layer prepared by a spin-coating process.

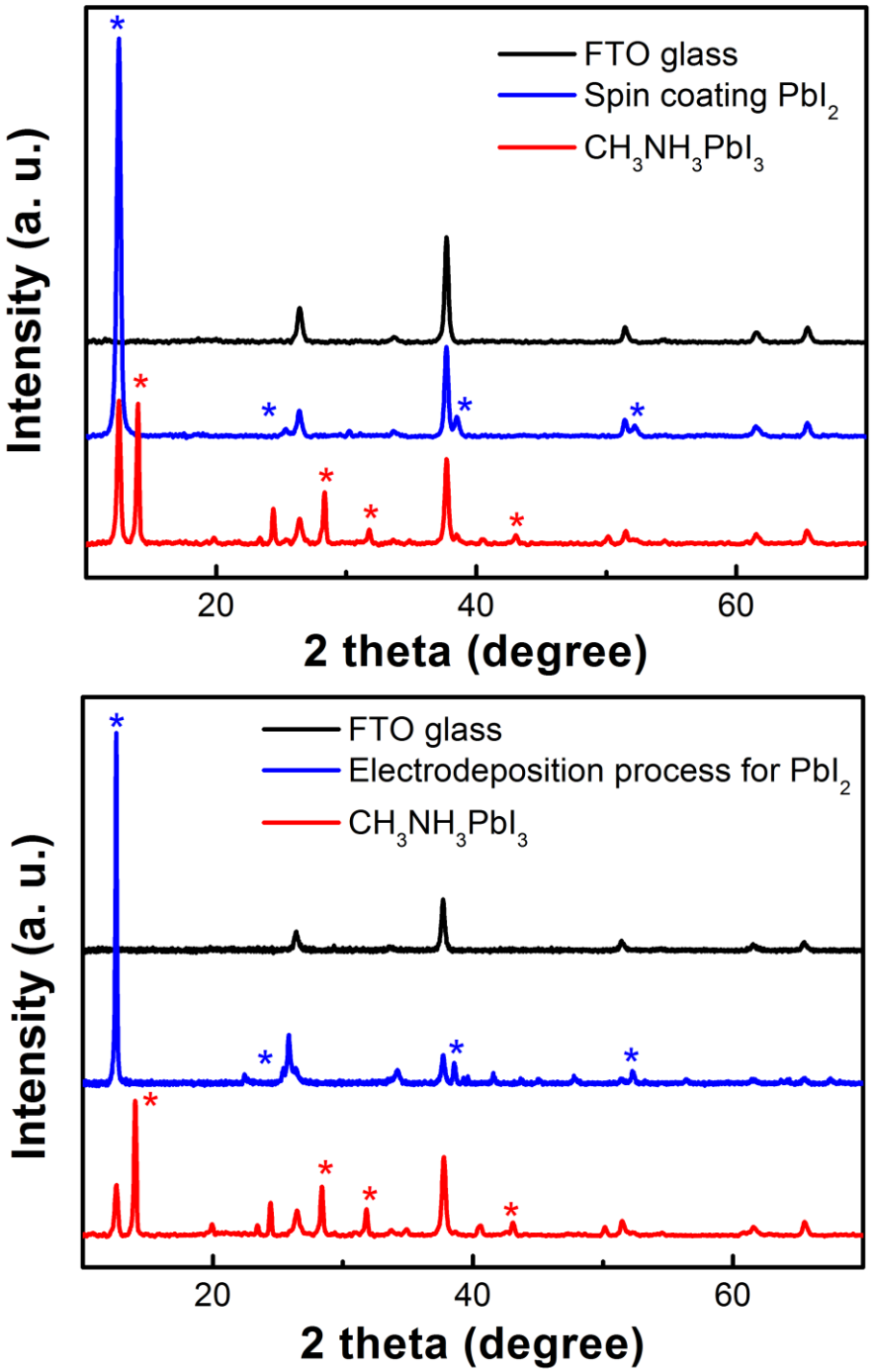

Figure S9. X-ray diffraction patterns of the perovskite layer prepared by two different coating processes during evolution. **a)** Spin-coating. **b)** Electrochemical deposition.

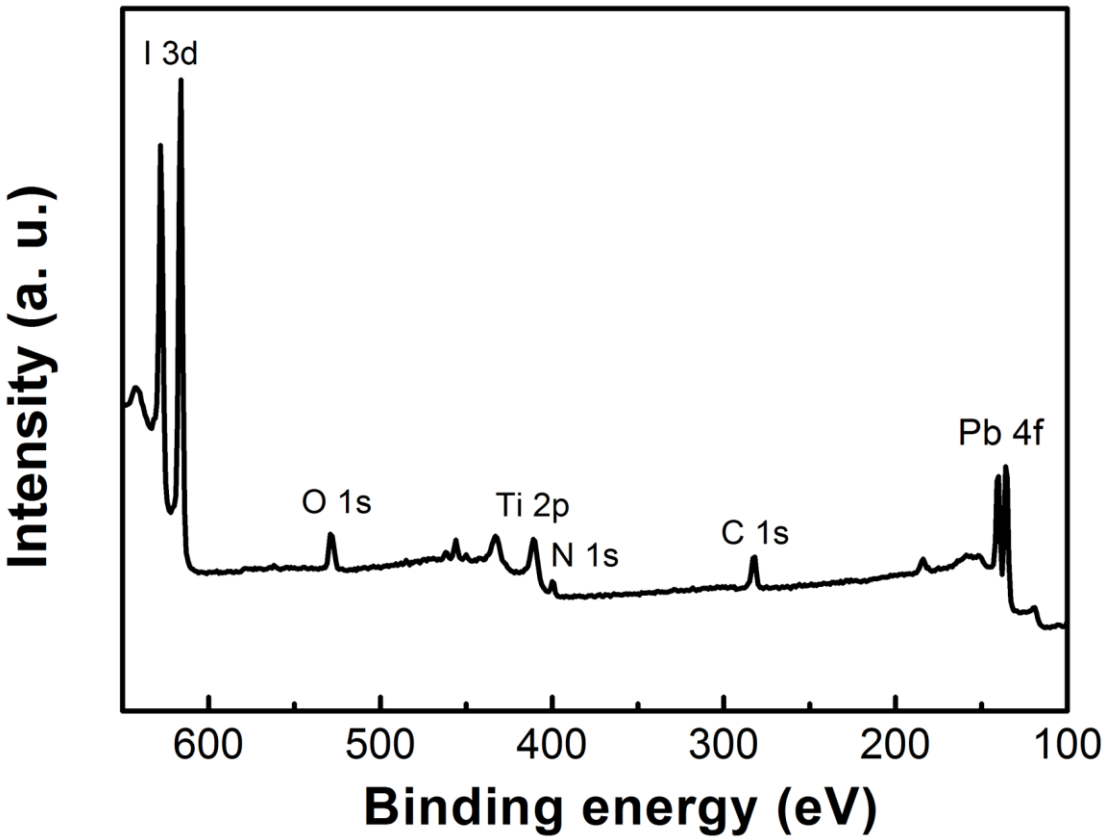

Figure S10. X-ray photoelectron spectroscopy analysis of the perovskite layer. The atomic ratios of N, Pb and I were 1/0.90/3.65.

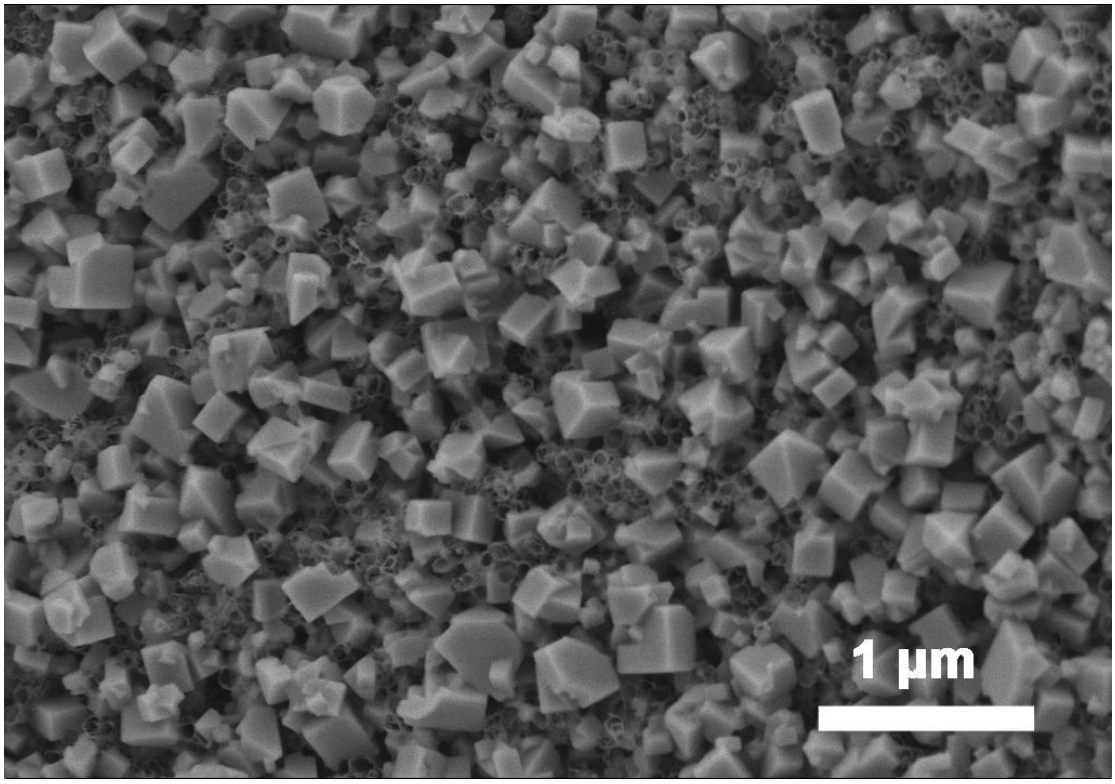

Figure S11. A low coverage of capping perovskite layer on the TiO_2 layer.

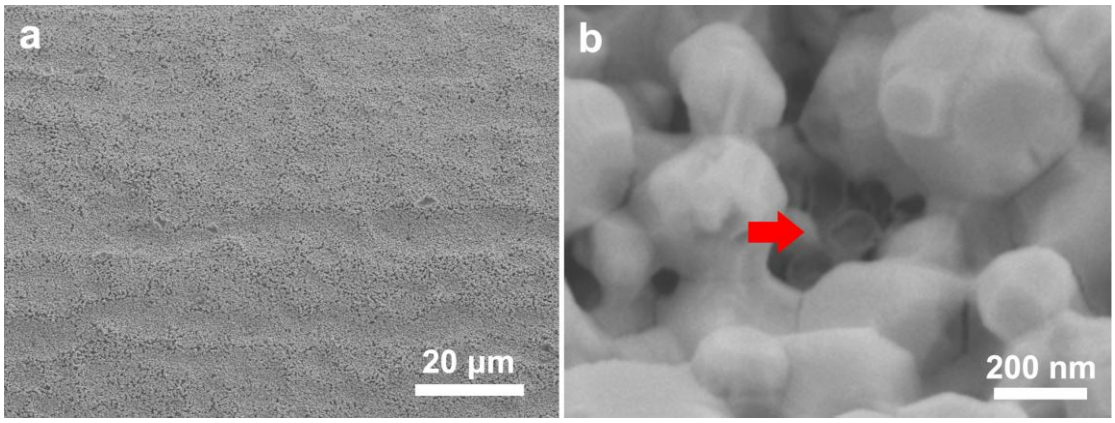

Figure S12. a) SEM image of a high surface coverage of perovskite layer with small pin-holes. **b**) TiO_2 nanotubes filled with light-harvesting and charge-generating perovskite materials.

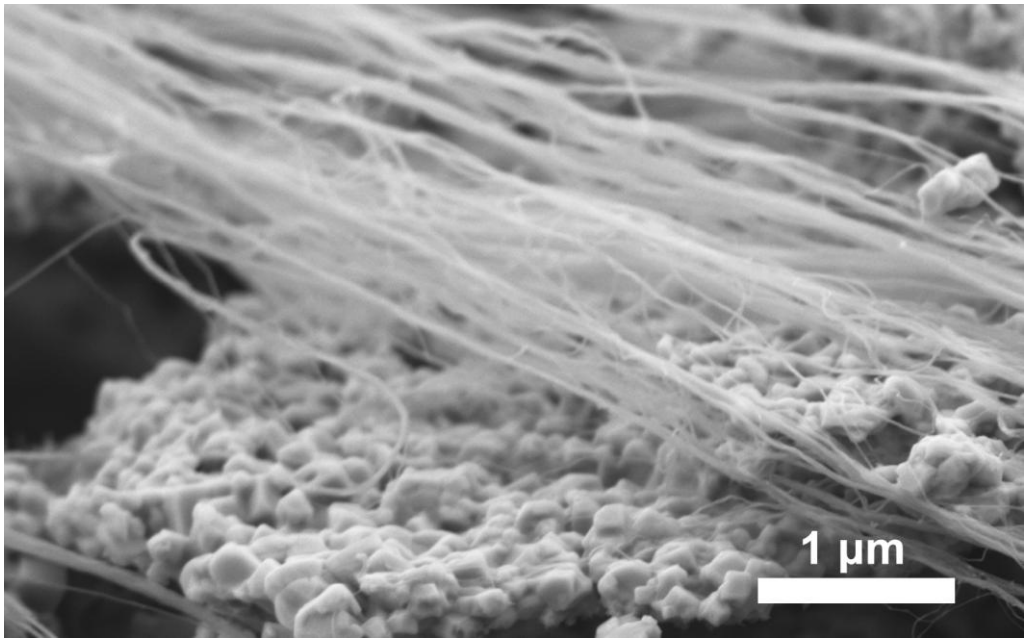

Figure S13. SEM image of a CNT sheet aerogel attached on the perovskite layer without isopropanol treatment.

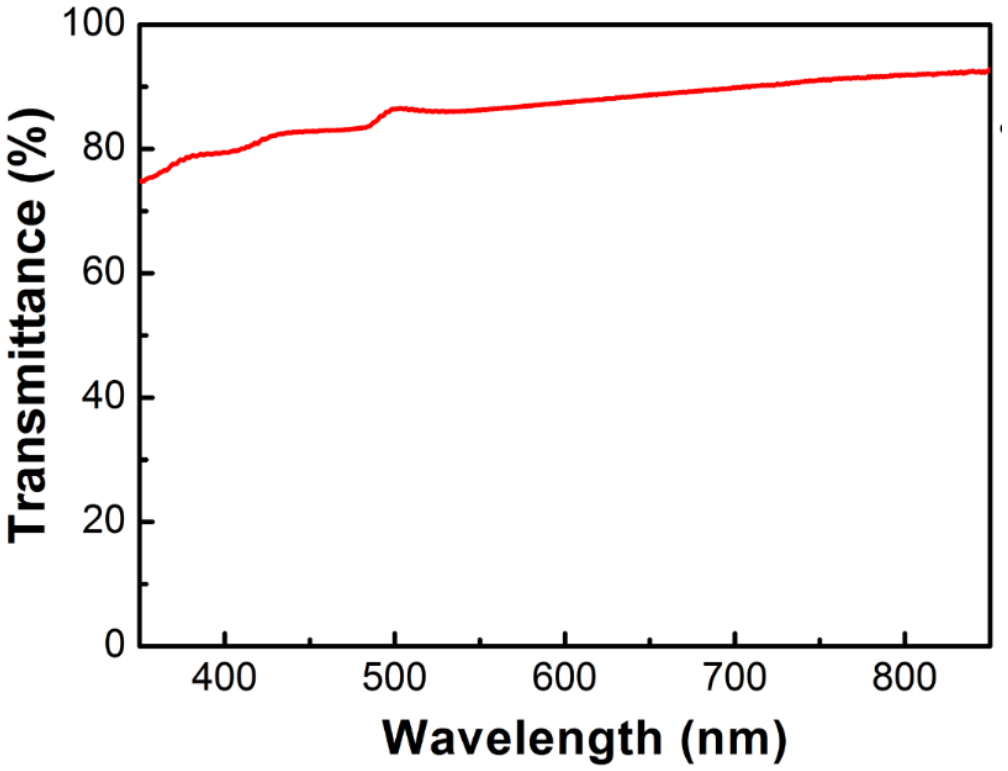

Figure S14. Dependence of transmittance on wavelength of a layer of CNT sheet.

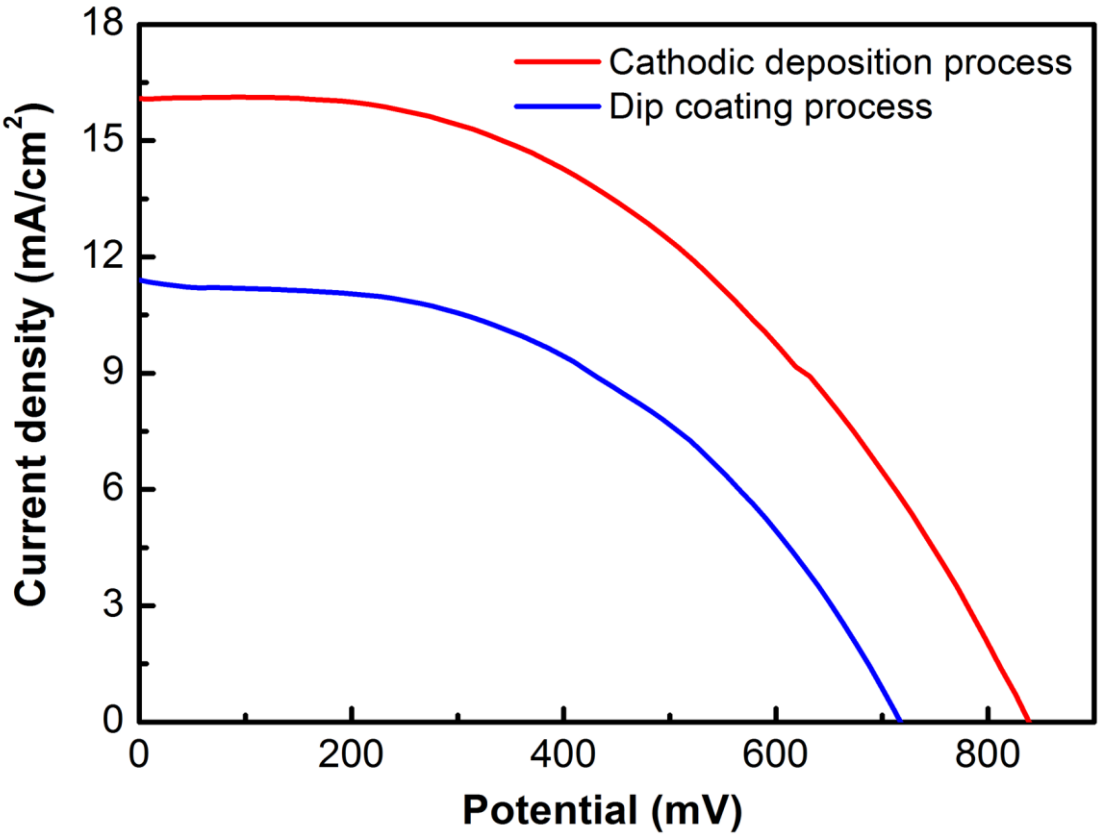

Figure S15. J-V curves of PSCFs fabricated by cathodic deposition and dip-coating processes.

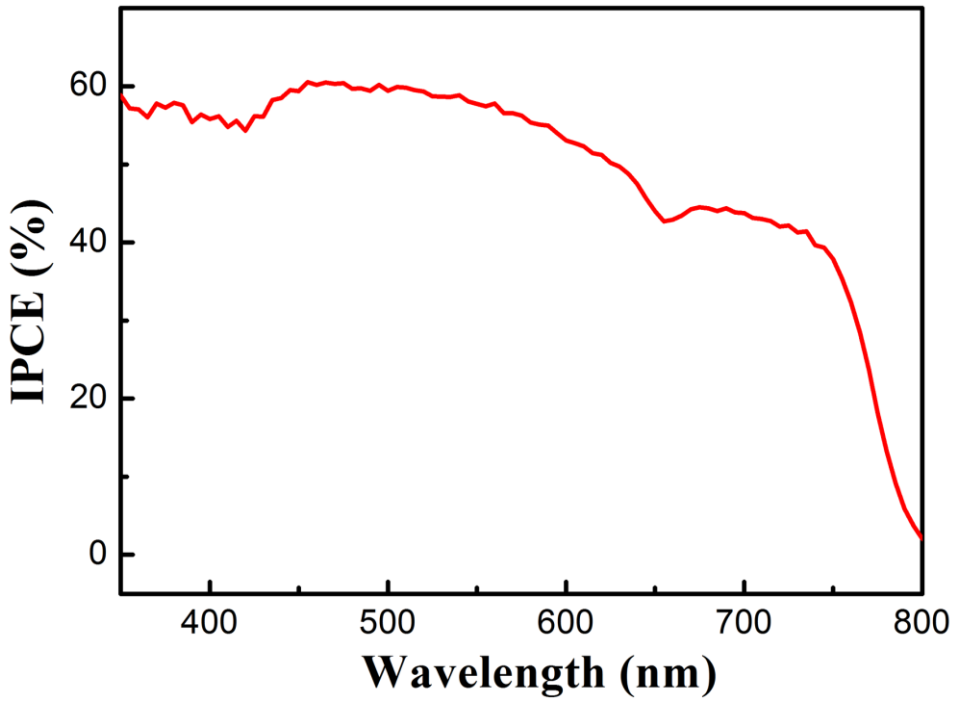

Figure S16. Typical EQE spectrum of the PSCF with a broad absorption.

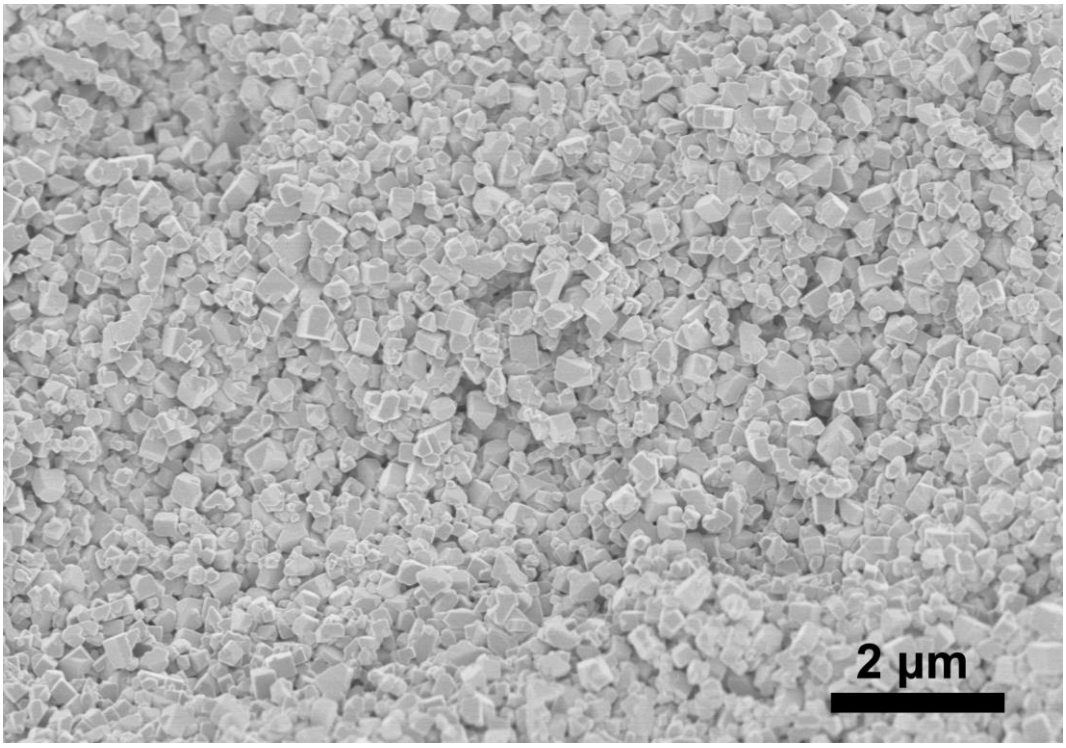

Figure S17. SEM image of a thicker perovskite layer.

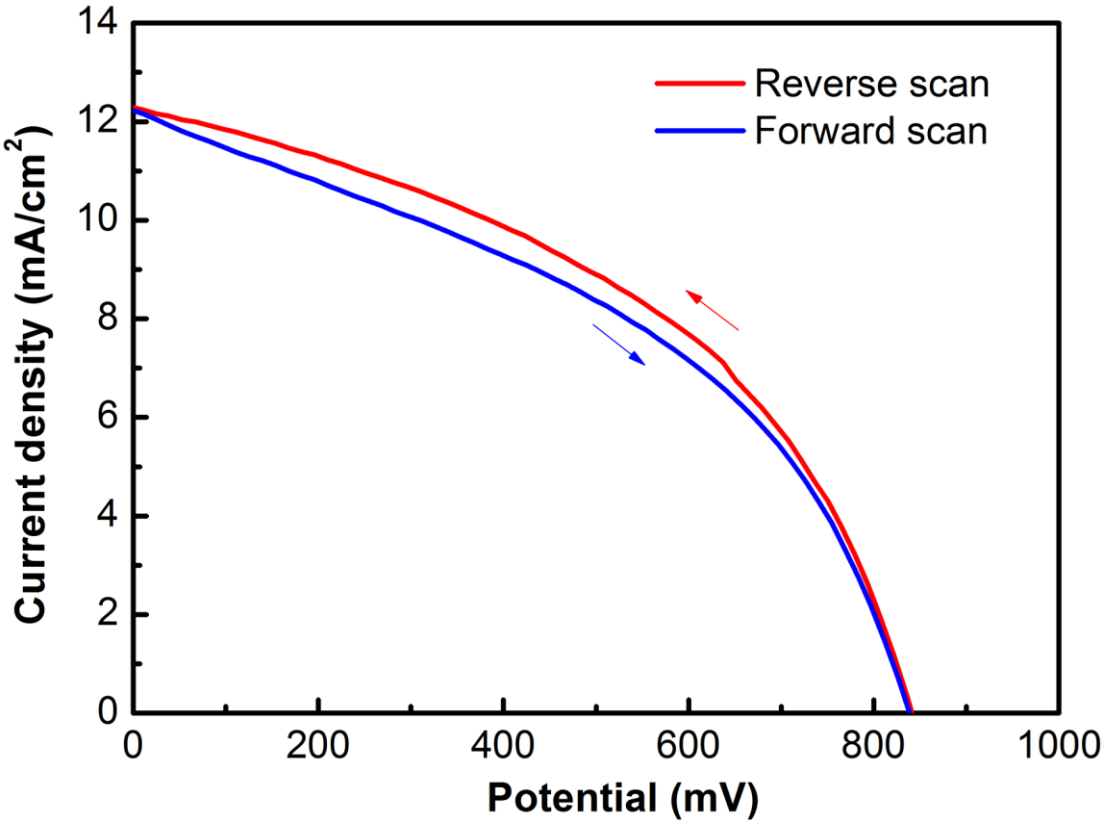

Figure S18. J-V curves of a PSCF under forward and reverse scans with a scan rate of 100 mV/s.

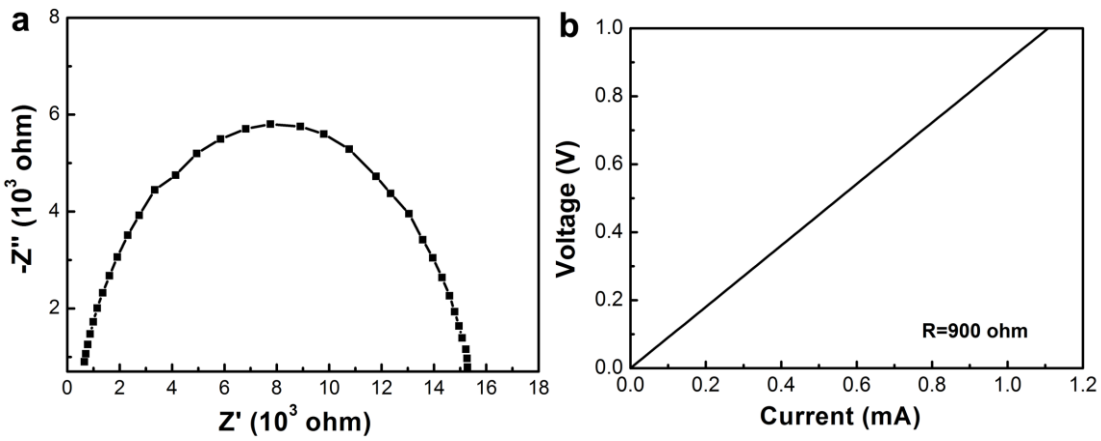

Figure S19. a) Electrochemistry impedance spectrum of a PSCF with aligned CNT sheet electrode. **b)** I-V curve of a CNT sheet electrode.

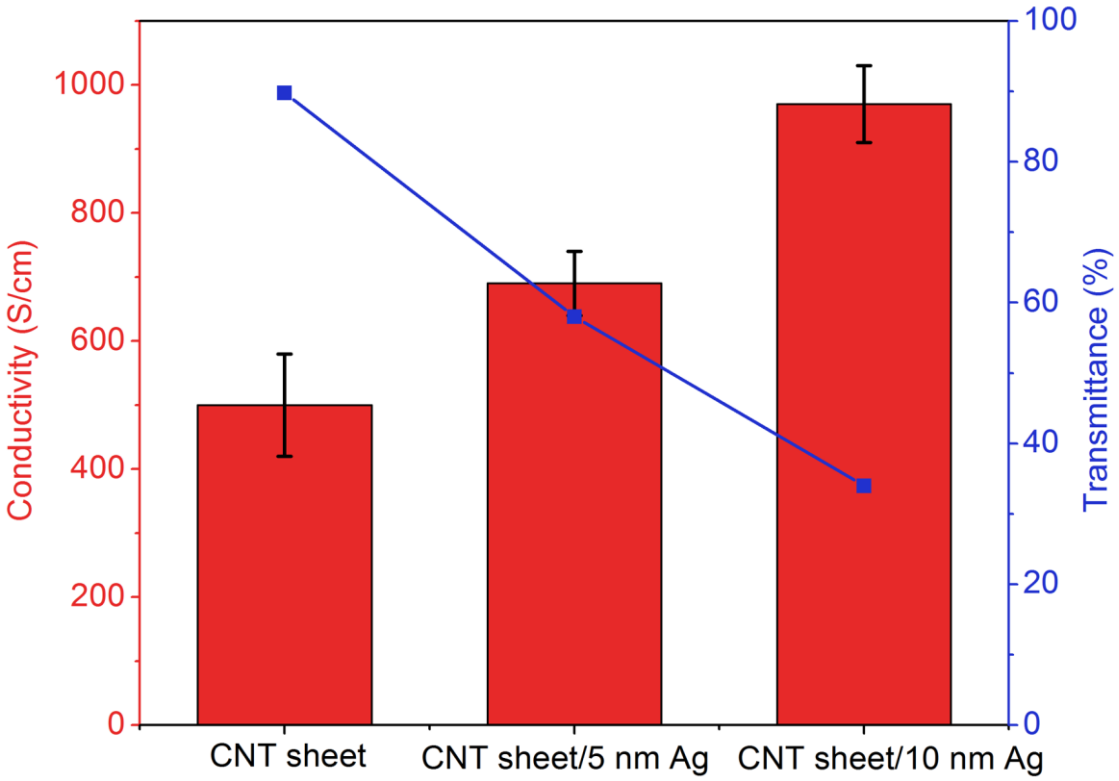

Figure S20. Electrical conductivity and optical transmittance at a wavelength of 600 nm for bare CNT sheet and CNT sheet/silver composites with the silver thickness of 5 and 10 nm.

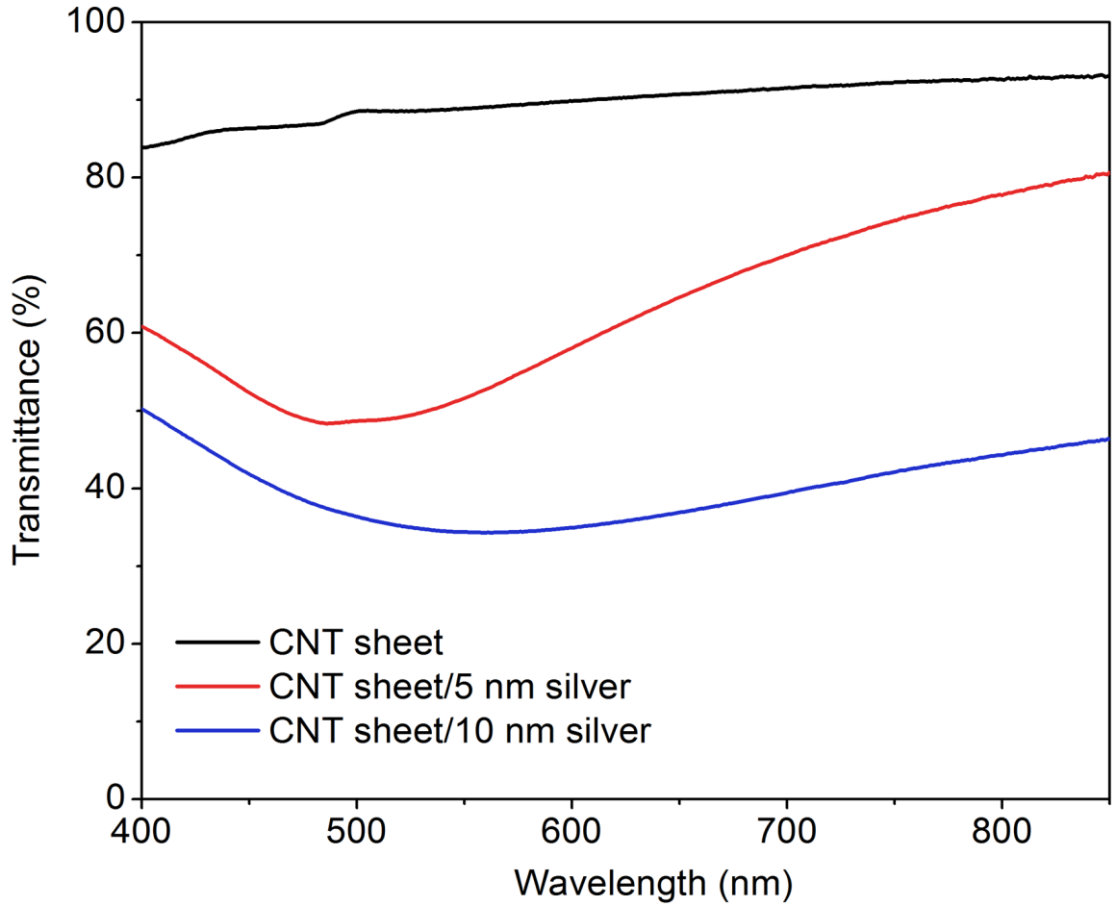

Figure S21. Transmittance spectra of bare CNT sheet and CNT sheet/silver composite films with the silver thickness of 5 and 10 nm at the wavelength range of 400 to 850 nm.

Figure S22. A long Ti wire that had been grown with an aligned TiO_2 nanotube array and deposited with a light-harvesting perovskite layer.

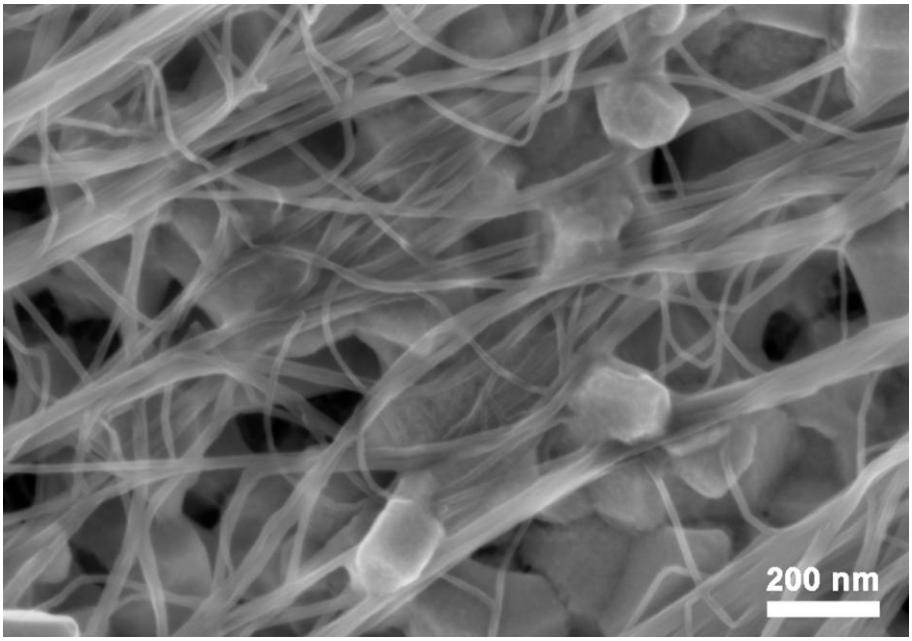

Figure S23. Aligned CNT sheet electrode coated with a perovskite layer being found to be stable after twisting.

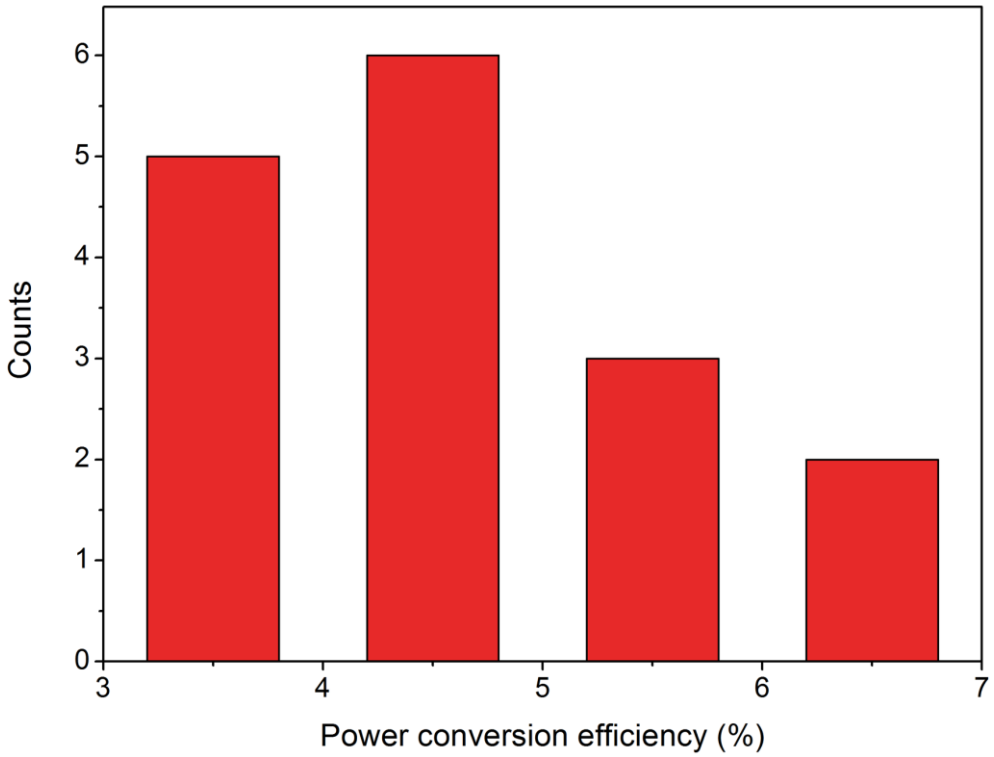

Figure S24. Histogram of the power conversion efficiencies for sixteen PSCFs fabricated from the perovskite layer with thickness of 350 nm.